Astron. Astrophys. 320, 1001–1012 (1997)

ASTRONOMY
AND
ASTROPHYSICS

Bisectors and line-parameter variations over granular and intergranular regions in 2-D artificial granulation

A.S. Gadun[1], **A. Hanslmeier**[2], **and K. N. Pikalov**[1]

[1] Main Astronomical Observatory of Ukrainian NAS, Goloseevo, 252650 Kiev-22, Ukraine
[2] Institut für Astronomie, Universitätsplatz 5, A-8010 Graz, Austria

Received 17 June 1996 / Accepted 13 September 1996

Abstract. Two sets of two-dimensional models of the solar granulation have been used to interpret the published observations of spectral lines of Fe I 4911.54, 4911.78, and 6494.99 Å obtained with high spectral and spatial resolution over selected granular and intergranular regions. The models differ by the horizontal size of the modeling region and treatment of thermal convection.

We study the variations of continuum intensity, residual intensity in the line cores, Doppler velocities, line asymmetries over granular and intergranular areas in the center of the solar disk and compare the correlation between these parameters obtained from models with observational ones.

A good reproduction of the observational results can be found only by applying 2-D models that treat the solar thermal convection as a fully non-stationary system with interacting flows. Such models also take into account the important role of secondary motions that influence the middle and upper photosphere. As essential perturbing factors there appear photospheric flows with supersonic velocities which can change the photometric profiles of granules, create regions with inversion of temperature distribution and impact onto the velocity field.

Variations of line parameters strongly depend on limitations in spatial resolution (spatial smearing). This was simulated in the models by applying different Gaussian smearing functions. Seeing was found to affect variations of equivalent widths, full widths at half maxima, and bisectors of the lines most strongly.

Key words: hydrodynamics – line: formation – Sun: granulation – Sun: photosphere

1. Introduction

The radiative-dynamic state of the solar photosphere, where the absorption lines are formed, is governed to a large degree by underlying convective unstable layers. A whole complex of motions in this region (turbulent, wave motions, overshooting convection) and inhomogeneities affect the spectral line profiles, causing their broadening, asymmetry, absolute shifts. The radiative-dynamic situation in the photosphere can be studied in detail by spectral observations with high spatial resolution and by direct numerical multidimensional modeling of the solar granulation including spectral observation simulations.

In this paper we make a direct and very detailed comparison between theoretical predictions and observational data obtained with high spatial resolution.

As observational basis we used data from the very detailed high quality spectral results which were obtained by Hanslmeier et al. (1994; hereafter Paper I) for Fe I lines: 4911.54 and 4911.78 Å with the 70-cm VTT Telescope at Izaña, Tenerife. In Paper I only three examples of the solar granulation picture are investigated which were specially preselected and, for this reason, Paper I data does not permit us to make a conclusion concerning the prevailing behaviour of spectral line parameters over granular and intergranular regions. Statistically more significant results were represented in papers of Nesis et al. (1992, 1993) for the Ni I 4912.03 Å line, but only for few line parameters. Finally, we also use observational conclusions from the paper by Hanslmeier et al. (1990, 1991) with spectral data from the smaller Gregory Coudé telescope and a different spectral range (about 6500 Å).

As computer simulations we considered two sets of time-dependent 2-D HD solar model atmospheres (Gadun 1995; Gadun & Pikalov 1996). They were computed with the same set of assumptions of numerical modeling of solar granulation (i.e., thermal convection at granular scales for approximating real solar conditions) but they differ by the treatment of thermal convection (as quasi-stationary or as full non-stationary) and by the horizontal sizes of modeling region. In all 2-D models there is a complete 2-D treatment of the radiation transfer. It includes the frequency dependence of the monochromatic continuum opacity (97 frequency points) and the radiation transfer in spectral lines using Kurucz's ODF tables (Kurucz 1979).

The obvious failing of such a category of models is the low Reynolds number (< 550 for the above mentioned models). This is far less than the values estimated for granulation scales

Send offprint requests to: A. Hanslmeier

(10^{10}–10^{13}). However, to obtain such large Re we have to choose a very small step in the spatial grid of the modeling region – close to the scale of viscosity dissipation (about several cm). That seems to be unrealizable at present. Nevertheless, it is very useful and important, to study the discrepancy between computed and observed data which might be affected by the overestimation of laminar flows in models.

We have to note that in the paper of Nesis et al. (1992) a qualitative interpretation of the spectral observations over granular fields was already given based on 2-D and 3-D HD models of Cattaneo et al. (1989) and Malagoli et al. (1990). This category of HD models is computed to study the behaviour of high-turbulent flows ($Re \sim 10^4$–10^6) for idealized cases without using real data concerning physical conditions in the solar envelope and atmospheric layers. Such a method of investigation does not permit direct comparisons with observations to be made, but give useful information to understand how low-turbulence flows change when they transfer to high-turbulence ones.

Recently, a study on the detection of shocks in the solar granulation has been carried out by Solanki et al. (1996). They used the observations of the Ni I 4912.03 Å line obtained with high spatial resolution near the solar disk center and close to its limb. The interpretation of such observations was done with the 2-D simulation of Steffen (Steffen & Freytag 1991).

In this paper the following basic conclusions were found: for the solar disk center, the enhancement of the line halfwidths cover the regions above downflows and do not coincide with the shock areas. So, Solanki et al. (1996) do not confirm the suggestion of Nesis et al. (1992) concerning the influence of transonic flows on the line broadening; for detection of shocks in the solar granulation they used observations close to the limb. In this case, above regions with the largest horizontal velocity gradients (including both areas with supersonic horizontal velocities and subsonic ones as well) the theoretical simulation predicts the line broadening. This is in good agreement with observations and may serve as one of the several methods for shock diagnostics.

2. 2-D models of solar granulation

The two sets of 2-D HD models used were described in detail by Gadun (1995), Gadun & Vorob'yov (1995), and Gadun & Pikalov (1996). Gadun (1996) considered the iron abundance determination based on these models. Below we will give some peculiarities of their computations which are important for the present investigations.

Both model sequences were computed with the mirror lateral boundary conditions. As we obtained from preliminary comparison of the HD models with the different treatment of the lateral boundary conditions (as mirror or periodical) the choice of type of the lateral boundary conditions does not influence to a strong degree on the present results but changes the flow topology and increases the number of the models with supersonic photospheric flows. The detailed analysis of the models with periodical lateral boundary conditions will be done in future papers.

The first set of 2-D HD models (Gadun 1995) describes only single granulation elements (single-scale approach, hereafter SS-models) as quasi-stationary cellular plane thermal convection. The rectangular modeling region had a size of 1295×2030 km in horizontal and vertical directions, the spatial step of the computational grid was 35 km. About 900 km in the model represents the atmospheric layers.

The theoretical Re is small for these models and may be estimated as $Re \sim (L/\Delta x)^{4/3} \sim 120$, where L is the horizontal size of the modeling region, Δx is the spatial step. But the real Reynolds number is still lower due to the influence of the numerical and approximated turbulent viscosity. Then the hydrodynamic excitations cannot give rise effectively to the multiplicity of turbulent vortices and such models have laminar flows in fact. So by analyzing these models we may investigate what observational data can be affected by laminar low-turbulent overshooting convection with quasi-column structure of vertical velocities in the photospheric layers. In other words this 2-D model describes the phenomenological classical conception concerning solar granulation as the upper part of convective flows which have the form of a mushroom or an umbrella.

The second set of 2-D HD models treats the thermal convection as non-stationary with interacting flows of different scales (multi-scale models, hereafter – MS-models). The size of their modeling region is 3990×2030 km and the spatial step of the computational grid is the same as in SS-models – 35 km. The upper limit of Re is 550. The secondary motions are very active in the upper part of model photospheres. They can affect on the granulation picture. Detailed studies of these models were carried out in several papers: the characteristics of artificial granules are given by Gadun & Vorob'yov (1995); the power spectra of 2-D granulation are represented by Gadun & Pikalov (1995); the results of application of such models to spectral analysis problems were obtained by Gadun (1996). These studies show that the MS-models more or less adequately reproduce the complex observed granulation features, but they still have their limitations.

Discussing such limitations we note, at first, that the models are two-dimensional. It means that mechanical motions are considered as planar loosing important information about the three-dimensional behaviour of inhomogeneities, the possible influence from vortex motions (Karpinsky 1990, Markov 1991, Nesis et al. 1993). Moreover, the spectrum of 2-D turbulence differs from 3-D one.

As follows from the analysis of power spectra and spectral line computations the influence of non convective origin model motions in the middle and upper model photosphere is larger than seen in observational data. They act on the overshooting convection lowering its photospheric level. Maybe this is due to lack of consideration of molecular lines in 2-D treatment of radiation transfer.

Table 1. List of using spectral lines

λ, Å	EPL, eV	d_{ob}	W_{ob}, mÅ	$log\ \tau_{5D}$	$log\ \tau_{5W}$	H_D, km	H_W, km
4911.536	4.26	0.27	24.	-1.05	-0.87	163	134
4911.782	3.96	0.49	44.	-1.37	-1.07	214	166
6494.994	2.40	0.75	162.	-4.16	-2.12	656	332

3. Synthesis of spectral lines

We computed 3 spectral lines of Fe I: 4911.54, 4911.78, and 6494.99 Å. In Table 1 we give their basic parameters: EPL is the excitation potential of the lower level in eV; W_{ob} and d_{ob} are the equivalent widths and central depths estimated relatively to the local continuum with the data of the Liège atlas (Delbouile et al. 1973); $\log \tau_{5W}$ and $\log \tau_{5D}$ are the depths of their formation at λ 5000 Å: the logarithm of the optical depth of formation of equivalent width weighted-mean over the whole profile and the logarithm of the effective optical depth of formation of the line center; H_W and H_D are effective geometrical heights of the formation of the whole profile and line center, respectively. The effective forming levels were calculated using the depression contribution function and the Unsöld–Pecker weight function with HOLMU model (Holweger & Müller 1974).

As is seen from Table 1, the first two lines are similar and they have close line formation heights. However, they are formed in the middle photosphere where we have overshooting convection and serve as a very sensible test to verify 2-D models. For that reason we have decided to include the results for both lines.

The line calculations were done in the LTE approximation for the center of the solar disk by a procedure described in Atroshchenko & Gadun (1994). The quantity Agf (abundance multiplied by oscillator strength) was chosen so that the correspondence between central depths was the best. From the sequence of SS-models we used 25 models with a temporal step of 30 s between the models. From the set of MS-models we took 529 models with the same temporal step. The topology of the flows in SS-models is seen to be stationary during the modeling time and the resulting spectral lines depend on the model oscillations only. For this reason the profiles of spectral lines after synthesis from SS-models were averaged over all 25 models and the final analysis of the line parameter variations was done based on these time-independent line profiles.

The limitation in spectral resolution was simulated by a convolution with a Gaussian having a dispersion of 20 mÅ. To simulate the spatial resolution we chose three spread functions:
1) $SF1$ is a sum of two Gaussians with dispersions: a_1 = 180 km and a_2 = 540 km. $SF1$ quite well describes the core of the real spread function (Deubner & Mattig 1975).
2) $SF2$ is the sum of two Gaussians too but with a_1 = 200 km and a_2 = 1500 km. Such a form of spread function is more preferable for taking into account the extended wings of the real spread function (Deubner & Mattig 1975).
3) $SF3$ is the sum of two Lorentzians with parameters a_1 = 180 km and a_2 = 1800 km. It considers the very extended wings of the real smearing function (Nordlund 1984).

Note, that all three spread functions were proposed to approximate the real spread function of the 40-cm Newton telescope at Izaña. The results of Paper I were found with another telescope. However we used the spread functions in the above mentioned forms because they allowed us to investigate the influence of finite resolution and seeing on the resulting predictions.

The equivalent widths (EW) and full widths at half maximum (line halfwidth – HW) were computed for the line profiles above each of the model vertical columns. The local continuum in each profile was taken as a continuum level.

The correlation coefficients for the line parameter variations were averaged over the whole horizontal size of the modeling region. So for SS-models such values apply to a single granule-intergranule area and for MS-models they are mean values over several (2–4) artificial granules.

4. Results for SS-models

An example of SS-model is shown in Fig. 1. The laminar character of photospheric flows, and the absence of perturbances in the upper photosphere are clearly seen. The photospheric velocity field is controlled by overshooting convection in fact. Figure 1d clearly also shows that the temperature fluctuations change their sign in the middle and upper photosphere. Such effect of negative correlation between photospheric vertical velocities and temperature fluctuations was obtained in numerous numerical experiments. It is explained by the rapid radiation cooling of hot upflows in the low photosphere and the warming of areas near downflows in the middle and upper photospheric layers affected by the compressing medium.

The line parameter variations and bisector shapes for Fe I 4911.78 and Fe I 6494.99 Å are given in Figs. 2 and 3. The values are plotted along the horizontal position above the modeling region. The data are computed directly from the models (without any smoothing) and with spectral and spatial smearing. Figures 1a–c depict the results for the weak Fe I 4911.54 Å line. They are plotted in brief form, because the variations of the missing parameters are qualitatively similar to that for the moderate line 4911.78 Å (Fig. 2). The results of the correlations are given in Table 2.

As is well known, the amplitudes of the variations are very sensitive to the effects of instrumental and atmospheric smearing. For instance, the initial relative rms fluctuations of intensity resulting from the model, decrease from $\sim$22% and $\sim$15% at $\lambda\lambda$ 4912 and 6495 Å to $\sim$6% and $\sim$4% after smoothing, respectively. They become close to the empirical values.

The character of line parameter variations is a function of different mechanisms of line formation and varying conditions in their forming levels. The most part of iron is ionized, only several percent are in neutral state under photospheric conditions. The Fe I lines prove to be very sensitive to model temperature as even relatively small variations in the temperature structure of the atmosphere cause substantial variations in the concen-

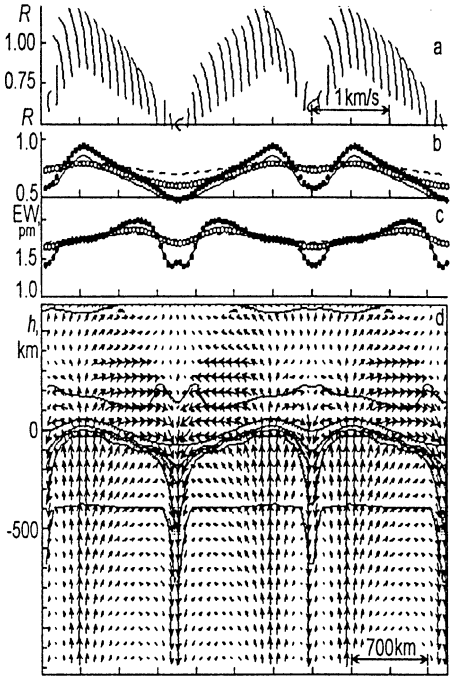

Fig. 1a–d. Weak Fe I 4911.54 Å line: the line parameter variations for SS-models (top), the typical velocity field and isotherms in SS-model (bottom). For convenience the modeling region and line parameter variations extended twice in horizontal direction in agreement with the lateral boundary conditions **a** The bisector shape without smoothing. **b** Variations of r – residual intensity in the line core. Solid lines are results obtained without smearing; dots are data after spectral smearing; circles are values after spatial smearing with $SF1$; dashed lines are simulation the largest spatial ($SF3$) smearing plus spectral smoothing. **c** Variations of EW – equivalent widths. Designations correspond to **b** **d** SS-model. Solid lines are isotherms for: 4000, 5000, 6000, 7000, 8000, 10000, and 12000 K (from top to bottom)

tration of neutral iron atoms. Moreover, the neutral iron atom concentrations are inversely proportional to the temperature. Due to the inverse distribution of the photospheric fluctuations, it means that the greatest concentration of the neutral iron atoms in the middle and upper photosphere is over granules.

Note should be taken that there is a transition zone between a positive and negative $< \delta T, \delta V >$ correlation, where δV are the horizontal variations of the vertical velocities and δT are the horizontal variations of the temperature. Both in 2-D and 3-D models (Gadun 1995) the temperature fluctuations change their sign near $\log \tau_R \sim -1$ (between 150–200 km). So the spectral lines which are formed above or under this conventional boundary should have a qualitatively different variation of parameters. Similar results were given by Stein and Nordlund (1989).

It should be pointed out too that the temperature distribution near the emitting layer in ascending and descending flows is radically different. The upflows (hot in subphotosphere) are characterized by very steep temperature gradients. In contrast to this downflows (more cool in subphotosphere) have a smooth change of the temperature. As a result, the lines formed above granules always have larger central depths than those resulting above intergranular lanes. This is clearly seen in Figs. 1, 2, and 3 from sizes of the line bisectors. A similar result was also obtained by Steffen (1989).

4.1. Variations of the residual intensity: δr

The variations of the residual intensity, δr, are given in Figs. 1b, 2f, and 3f. Observing weak lines this parameter reflects the spatial variations of continuum intensity which are located near the transition zone where the temperature fluctuations change their sign while in strong lines it indicates the distribution of selectively absorbing agents and the contribution is mainly from the middle-upper photosphere where the temperature fluctuations are already inverse.

Weak Fe 4911.54Å line: we find a high correlation $< \delta i, \delta r >$ = 0.96 without smearing. The intensity fluctuations in the core are less than in the continuum. A weak negative $< \delta T, \delta i >$ (or $< \delta T, \delta V >$) correlation in the line core formation level was found. Therefore at the level of line core formation the temperature fluctuations which can be associated with the intensity fluctuations, are less than at the level of the continuum.

Moderate Fe I 4911.78 Å line: this tendency becomes stronger and δr (Fig. 2f) already differs from δi (Fig. 2e). These differences are caused by increasing the negative correlation $< \delta T, \delta i >$ (or $< \delta T, \delta V >$) and are localized around intergranular areas, where in the middle photosphere the temperature increases in comparison with the nearest granular regions. The correlation $< \delta i, \delta r >$ decreases to 0.58, the rms intensity fluctuations in the line core also reduce.

Strong line Fe I 6494.99 Å: the contribution of the proper line emission to the resulting δr is the largest. So δr depends on the distribution of selectively absorbing agents in the middle and upper photosphere and hence on the temperature distributions in these layers. As a result, the correlation of $< \delta i, \delta r >$ becomes negative, reflecting the inversion character of the temperature fluctuations. δr well correlates with variations of the Doppler velocities $< \delta v, \delta r >$ showing that the upflows are coolest in the upper photospheric layers.

4.2. Variations of the equivalent width (δEW)

δEW values are given in Fig. 1c, 2h, and 3h. The basic factors influencing EW values are:

1) as it was mentioned above due to the steeper temperature gradient in the hot granular upflows the Fe I lines always have deeper line profiles and respectively larger EW above the granules;

2) EW values are affected by the concentration of selectively absorbing agents in the line forming region. So EW depends on the temperature distribution in these layers;

3) EW is changed due to the broadening by non-thermal velocities.

These factors are well seen in our line sample. All three lines demonstrate the EW enhancement above granules and EW drops above the intergranular regions.

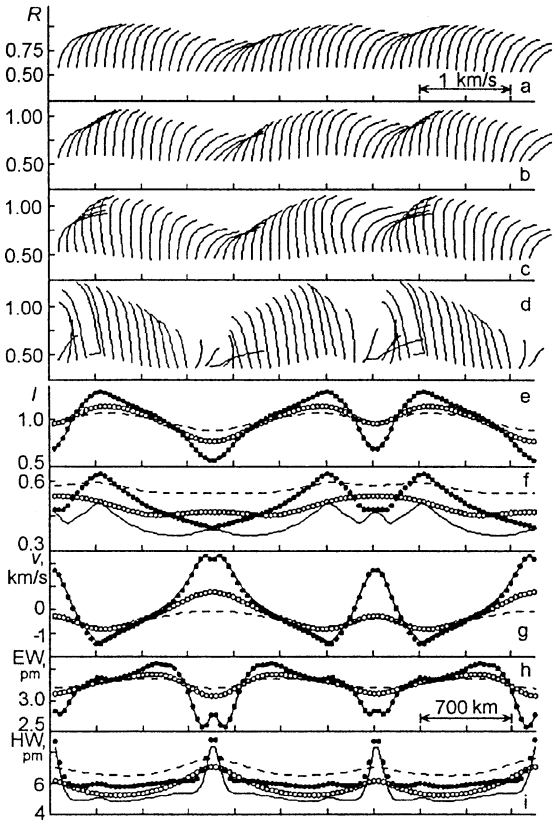

Fig. 2a–i. Moderate Fe I 4911.78 Å line: the line parameter variations for SS-models. For convenience the line parameter variations were twice extended in horizontal direction in agreement with lateral boundary conditions in modeling. **a** The bisectors after spectral and spatial ($SF3$) smearing. **b** The bisectors after spectral and spatial ($SF2$) smearing. **c** The bisectors after spatial ($SF1$) smearing. **d** The bisectors without smoothing. **e** Continuum intensity variations (δi). Designations correspond to Fig. 1b. **f** Line core intensity variations (δr). Designations correspond to Fig. 1b. **g** Doppler velocities (δv). Designations correspond to Fig. 1b. **h** Equivalent widths variations (δEW). Designations correspond to Fig. 1b. **i** Line halfwidths variations (δHW). Designations correspond to Fig. 1b.

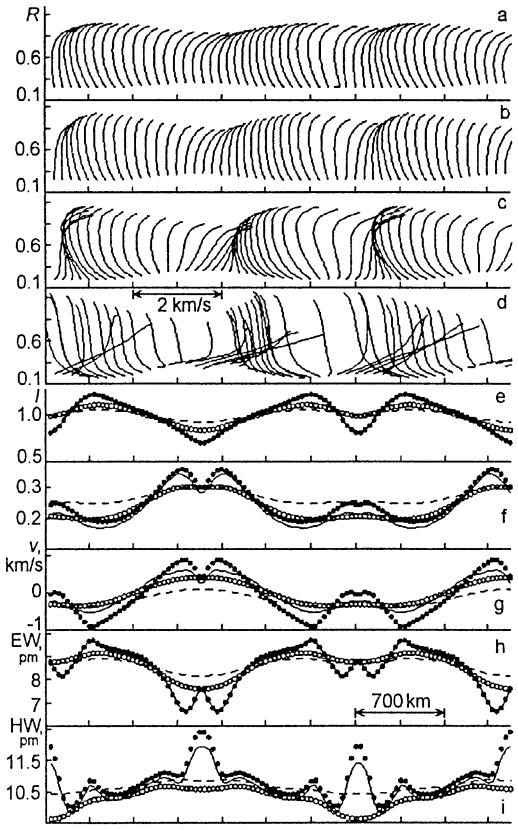

Fig. 3a–i. Strong Fe I 6494.99 Å line: the line parameter variations for SS-models. For convenience the line parameter variations were twice extended in horizontal direction in agreement with lateral boundary conditions in modeling. Designations and plotting order correspond to Fig. 2.

Weak line Fe I 4911.54 Å: the variations of selectively absorbing agents across the upflow regions change the shape of the δEW curve above the granule. The broadening by non-thermal velocities seems to be small (Fig. 1c).

Moderate line Fe I 4911.78 Å: qualitatively, the EW variations are close to that which were obtained for Fe I 4911.54 Å line. However, the influence of non-thermal velocities on EW (Fig. 2h) is obvious.

Strong Fe I 6494.99 Å line: the δEW (Fig. 3h) show high anticorrelation with $\delta r - < \delta EW, \delta r > = -0.91$. It is explained by the similar mechanisms impacting on their values. The influence of non-thermal velocities is seen clearly.

4.3. Variations of the Doppler velocities (δv)

The δv for moderate and strong Fe I lines are plotted in Figs. 2g and 3g, respectively. The results for Fe I 4911.54 Å are not shown here because they are qualitatively similar to those in Fig. 2g. δv reflects the character of vertical velocities in the line core forming region. The photospheric velocity field in SS-models is defined by the laminar overshooting convection. So the δv curves are similar for all three lines. The differences can be seen above intergranular regions. The amplitudes of δv are also changed: for the strongest line they are 2 times smaller than for the weakest one.

4.4. Variations of the line halfwidth (δHW)

The variations of the full width at half line maximum (hereafter δHW) are shown in Figs. 2i and 3i for moderate and strong lines: 4911.78 and 6494.99 Å, respectively. Data for 4911.54 Å are not given because they qualitatively are similar to Fig. 2i. HW values are a function of line-of-sight velocity gradients in the line forming region. For weak and moderate lines such gradients are very similar. More essential discrepancies may be pointed for the strong line because its height range of formation occupies the whole photosphere. The highest peaks on the δHW curves were found above downflows, less pronounced ones cover the areas above center of upflow

and near the maxima of horizontal velocities. All these peaks are more conspicuous in the computation of the strong line.

4.5. The influence of spatial and spectral smearing on line parameter variations

As it is seen from the results, the spectral smoothing does not qualitatively change the properties of the line parameter variations. The spatial smearing essentially affects on the amplitudes of variations. Examples of this can be seen in Fig. 2f and 3i.

The shape of bisectors also essentially depends on the spatial averaging. The bisectors obtained directly from SS-models show the well known blue (in the case of granules) and red asymmetries (in the case of intergranules). The red asymmetries are larger than the blue asymmetries because the downflow is concentrated into smaller areas and has larger velocity gradients. For the higher forming line Fe I 6494.99 Å this effect is most pronounced. This has been studied e.g. by Steffen (1989).

As a cumulative effect of poorer spatial resolution the asymmetries are decreased (Steffen 1989). Moreover, the lines with the widest profiles are formed above intergranular regions in our models. They are affected more strongly by the smearing and the smoothed resulting profiles have red asymmetries in the line wings.

4.6. Correlation coefficients and comparison with observations

As it follows from Table 2 the values of the correlation coefficients for weak and moderate lines are more affected by the smearing effects than for the strong one. As a common peculiarity we may note high values of some correlation coefficients – higher than found from observations.

Weak line: the correlations $< \delta i, \delta r >$, $< \delta i, \delta v >$, and $< \delta v, \delta r >$ are not much affected by a simulation of decreasing spatial and spectral resolution and are similar to the observations (Paper I). The correlations with δHW and especially δEW are affected by smoothing very strongly. Allowing for the change of amplitudes of δEW correlations, depending on the spread functions, we may suppose that the δEW correlation coefficients do not contradict observations (Paper I). But correlations with δHW do not agree with the observations (Paper I) and taking into account the smoothing this does not increase the agreement. Three pictures of the granulation field, which are shown in Paper I, demonstrate the HW enhancement between minimum and maximum of line-of-sight velocities and variations of continuum intensity. SS-models only give the HW enhancement above intergranular lanes at regions with the minimum of v and i.

Moderate line: similar to the above mentioned case. The correlations $< \delta i, \delta r >$, $< \delta i, \delta v >$, and $< \delta v, \delta r >$ qualitatively agree with observational examples (Paper I). Again correlations with δHW contradict observational ones when any smoothing is performed.

Strong line: from SS-models we obtained the high values for the bulk of coefficients, especially for $< \delta EW, \delta r >$ and $< \delta v, \delta r >$. For $< \delta i, \delta r >$ and $< \delta v, \delta r >$ we found opposite dependencies in comparison with weaker lines. The causes of this were discussed above.

Table 2. Correlation coefficients and rms intensity fluctuations in continuum and line cores. SS-models

Correlations	$Without\ smearing$	$Smearing\ only\ spectral$	$Spatial\ only$ SF1	$Spatial\ only$ SF2	$Spatial + spectral$ SF3
		4911.54Å			
$< \delta i, \delta v >$	−0.99	−0.99	−0.98	−0.95	−0.97
$< \delta v, \delta HW >$	0.71	0.71	0.87	0.80	0.83
$< \delta v, \delta EW >$	−0.60	−0.60	0.03	−0.05	0.10
$< \delta v, \delta r >$	−0.93	−0.96	−0.97	−0.97	−0.99
$< \delta i, \delta HW >$	−0.68	−0.68	−0.92	−0.93	−0.93
$< \delta i, \delta EW >$	0.54	0.54	0.11	0.32	0.11
$< \delta i, \delta r >$	0.96	0.98	0.93	0.90	0.97
$< \delta HW, \delta EW >$	−0.67	−0.67	−0.45	−0.55	−0.41
$< \delta HW, \delta r >$	−0.51	−0.59	−0.75	−0.73	−0.83
$< \delta EW, \delta r >$	0.31	0.39	−0.22	−0.10	−0.12
$\Delta I_{\rm rms}^{cont.}, \%$	22.0	22.0	11.9	8.5	5.9
$\Delta I_{\rm rms}^{line}, \%$	17.8	19.3	9.1	5.4	4.7
		4911.78Å			
$< \delta i, \delta v >$	−0.99	−0.99	−0.98	−0.97	−0.97
$< \delta v, \delta HW >$	0.72	0.72	0.92	0.85	0.87
$< \delta v, \delta EW >$	−0.74	−0.75	−0.44	−0.45	−0.36
$< \delta v, \delta r >$	−0.56	−0.88	−0.52	−0.09	−0.85
$< \delta i, \delta HW >$	−0.73	−0.72	−0.96	−0.95	−0.95
$< \delta i, \delta EW >$	0.72	0.72	0.54	0.64	0.53
$< \delta i, \delta r >$	0.58	0.90	0.41	−0.12	0.74
$< \delta HW, \delta EW >$	−0.64	−0.65	−0.73	−0.77	−0.73
$< \delta HW, \delta r >$	−0.09	−0.49	−0.19	0.31	−0.53
$< \delta EW, \delta r >$	−0.05	0.39	−0.49	−0.82	−0.15
$\Delta I_{\rm rms}^{cont.}, \%$	22.0	22.0	11.9	8.5	5.9
$\Delta I_{\rm rms}^{line}, \%$	10.7	13.8	6.3	4.3	3.1
		6494.99Å			
$< \delta i, \delta v >$	−0.74	−0.90	−0.87	−0.83	−0.97
$< \delta v, \delta HW >$	0.62	0.62	0.83	0.71	0.87
$< \delta v, \delta EW >$	−0.79	−0.93	−0.91	−0.88	−0.98
$< \delta v, \delta r >$	0.94	0.98	0.99	0.97	0.98
$< \delta i, \delta HW >$	−0.77	−0.79	−0.49	−0.22	−0.74
$< \delta i, \delta EW >$	0.89	0.89	0.98	0.98	0.99
$< \delta i, \delta r >$	−0.82	−0.86	−0.92	−0.91	−0.94
$< \delta HW, \delta EW >$	−0.58	−0.57	−0.58	−0.32	−0.80
$< \delta HW, \delta r >$	0.62	0.62	0.77	0.58	0.91
$< \delta EW, \delta r >$	−0.91	−0.94	−0.95	−0.95	−0.97
$\Delta I_{\rm rms}^{cont.}, \%$	15.3	15.3	8.6	6.0	4.3
$\Delta I_{\rm rms}^{line}, \%$	25.4	22.7	17.5	11.2	7.8

We compare the obtained values with the observational data of Hanslmeier et al. (1990) for several correlation coefficients which were found over a large statistics of granules. The theoretical data obtained differ very strongly from observational ones as a result of absent secondary motions in these models.

So, the analyzed SS-models cannot reproduce the observational examples of granulation fields in adequate form. They give too high amplitudes of the correlation coefficients in comparison with the observational values (Paper I, Hanslmeier et al. (1990)). Especially drastic discrepancies can be found when analyzing the variations of the line halfwidths. Moreover, the data from Paper I clearly show the examples of blue line asymmetry at regions with downflows. This is also excluded by SS-models. SS-models are well known not to reproduce the observations (e.g. Steffen 1991). However, in this context we wanted to stress the low agreement with observations between the correlations of all other line parameters and the equivalent width.

5. Results for MS-models

The flow topology and the radiative-dynamic situation in the photospheric layers of these models are strongly time-dependent. So, the line parameter variations and correlations also depend on the time. An example of time-dependent variations of $< \delta i, \delta v >$ for FeI 4911.78 Å is shown in Fig. 4:

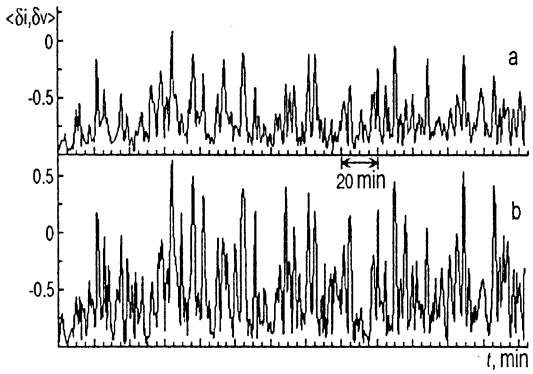

Fig. 4a and b. Time-dependent variations of $< \delta i, \delta v >$ for Fe I 4911.78 Å computed with MS-models. **a** The results is obtained without smoothing. **b** The values is obtained with spectral and spatial ($SF3$) smearing.

a) when the values were obtained without any smoothing and b) with a simulation of spectral and spatial smearing (by $SF3$).

The correlation coefficients averaged over 529 models are given in Table 3. For two cases when the results are free from smearing and when the decrease of spectral and spatial resolution are the largest ($SF3$ smearing function plus spectral smoothing), we show the minimum and maximum of corresponding correlations.

As it follows from Fig. 4 and Table 3 the amplitude of time-dependent correlations is high and increases after smearing up to 1.94 for some correlations (values are not normalized). Maybe, such time-dependent behaviour of the correlations is caused by an overestimated amplitude of the model oscillations.

The presence of the secondary motions in the photospheric layers decreases the correlations which were found with laminar overshooting convection (compare Table 2 and 3). Please also note the higher values of intensity fluctuations in the continuum and line cores in comparison with SS-models. As was the case in the SS-models, taking into account the decreasing spectral and spatial resolution, changes the correlation coefficients.

Weak 4911.54 Å line: only the absolute values of three correlation coefficients ($< \delta i, \delta r >$, $< \delta i, \delta v >$, and $< \delta v, \delta r >$) are above 0.5. This is in qualitative agreement with observational results (Paper I). However, in Paper I a high correlation of $< \delta HW, \delta r >$ was obtained. The averaged time-dependent correlations contradict this observational result.

Moderate 4911.78 Å line: from the three coefficients ($< \delta i, \delta r >$, $< \delta i, \delta v >$, and $< \delta v, \delta r >$) only $< \delta i, \delta v >$ has a high negative value. This does not agree with Paper I and the results obtained for SS-models. It may be interpreted by an essential influence of the secondary motions in the line forming region. Because the observations (Paper I) do not show such strong differences between weak and moderate lines, we may suppose that the MS-modeled overshooting convection has a slightly drowned nature in comparison with SS-models. This conclusion is also confirmed by the high value of relative intensity fluctuations in the line core (Table 3) which are close to those in the continuum. For SS-models they were about 2 times smaller than continuum intensity fluctuations. We can also note the increased anticorrelation between EW and r.

Table 3. Correlation coefficients and rms intensity fluctuations in continuum and line cores. MS-models

Correlations	$Without$ $smearing$			$Smearing$ $without$ SF1	$spatial$ $spectral$ SF2	$spatial$ $+spectral$ SF3		
				4911.54Å				
$< \delta i, \delta v >$	−0.73	− 0.96	0.00	−0.59	−0.54	−0.54	− 0.98	0.62
$< \delta v, \delta HW >$	0.38	− 0.58	0.86	0.50	0.47	0.41	− 0.94	0.98
$< \delta v, \delta EW >$	−0.24	− 0.92	0.78	0.07	0.17	0.19	− 0.95	0.96
$< \delta v, \delta r >$	−0.60	− 0.94	0.38	−0.47	−0.41	−0.50	− 0.98	0.81
$< \delta i, \delta HW >$	−0.48	− 0.88	0.71	−0.61	−0.63	−0.58	− 0.98	0.55
$< \delta i, \delta EW >$	0.19	− 0.76	0.91	−0.01	−0.03	−0.06	− 0.95	0.93
$< \delta i, \delta r >$	0.88	− 0.11	0.98	0.78	0.74	0.85	− 0.43	0.99
$< \delta HW, \delta EW >$	−0.09	− 0.69	0.63	−0.36	−0.36	−0.38	− 0.98	0.90
$< \delta HW, \delta r >$	−0.29	− 0.79	0.81	−0.16	−0.12	−0.21	− 0.96	0.88
$< \delta EW, \delta r >$	−0.20	− 0.88	0.70	−0.50	−0.54	−0.44	− 0.97	0.85
$\Delta I_{\rm rms}^{cont.}$, %		24.3		15.9	11.5		8.4	
σ		4.4		4.5	3.5		2.7	
$\Delta I_{\rm rms}^{line}$, %		23.0		15.8	11.4		8.3	
σ		5.7		5.9	4.8		3.3	
				4911.78Å				
$< \delta i, \delta v >$	−0.69	− 0.96	0.09	−0.57	−0.52	−0.53	− 0.97	0.64
$< \delta v, \delta HW >$	0.33	− 0.79	0.90	0.57	0.56	0.50	− 0.95	0.99
$< \delta v, \delta EW >$	−0.29	− 0.92	0.80	−0.00	0.08	0.12	− 0.91	0.95
$< \delta v, \delta r >$	−0.11	− 0.84	0.79	−0.07	−0.02	−0.23	− 0.98	0.94
$< \delta i, \delta HW >$	−0.50	− 0.91	0.82	−0.68	−0.69	−0.65	− 0.98	0.57
$< \delta i, \delta EW >$	0.29	− 0.78	0.91	0.10	0.07	0.04	− 0.95	0.93
$< \delta i, \delta r >$	0.28	− 0.71	0.87	0.15	0.09	0.39	− 0.92	0.96
$< \delta HW, \delta EW >$	0.11	− 0.64	0.84	−0.23	−0.26	−0.32	− 0.96	0.92
$< \delta HW, \delta r >$	−0.07	− 0.81	0.77	0.24	0.36	0.19	− 0.94	0.98
$< \delta EW, \delta r >$	−0.65	− 0.97	0.23	−0.81	−0.81	−0.73	− 0.99	0.56
$\Delta I_{\rm rms}^{cont.}$, %		24.3		15.9	11.5		8.4	
σ		4.4		4.5	3.5		2.7	
$\Delta I_{\rm rms}^{line}$, %		24.2		20.8	15.7		9.7	
σ		7.1		7.4	6.3		4.0	
				6494.99Å				
$< \delta i, \delta v >$	−0.17	− 0.91	0.71	−0.18	−0.15	−0.25	− 0.96	0.82
$< \delta v, \delta HW >$	−0.07	− 0.81	0.83	0.07	0.14	0.19	− 0.94	0.98
$< \delta v, \delta EW >$	0.00	− 0.76	0.77	0.04	0.06	0.05	− 0.91	0.95
$< \delta v, \delta r >$	−0.10	− 0.88	0.74	−0.06	−0.05	−0.01	− 0.95	0.95
$< \delta i, \delta HW >$	−0.13	− 0.88	0.85	−0.33	−0.40	−0.47	− 0.98	0.96
$< \delta i, \delta EW >$	0.27	− 0.79	0.89	0.14	0.10	0.09	− 0.95	0.96
$< \delta i, \delta r >$	−0.23	− 0.79	0.72	−0.31	−0.27	−0.30	− 0.94	0.70
$< \delta HW, \delta EW >$	0.41	− 0.79	0.94	0.34	0.30	0.29	− 0.94	0.98
$< \delta HW, \delta r >$	0.18	− 0.66	0.90	0.26	0.30	0.31	− 0.83	0.98
$< \delta EW, \delta r >$	−0.66	− 0.97	0.36	−0.67	−0.66	−0.67	− 0.99	0.66
$\Delta I_{\rm rms}^{cont.}$, %		16.9		11.5	8.3		6.1	
σ		3.4		3.5	2.8		2.1	
$\Delta I_{\rm rms}^{line}$, %		54.9		37.8	26.7		18.1	
σ		16.1		12.1	9.0		6.3	

Strong Fe I 6494.99 Å line: in contrast to the SS-model results there is a high anticorrelation only between $< \delta EW, \delta r >$. The low other correlations could be caused by the strong influence of the stochastic (oscillatory) motions in the line forming region – in the middle and upper photosphere. This is confirmed by very high intensity fluctuations in the line core: they are higher ($\sim$2) than in the case of the corresponding SS-model results. Maybe, such a strong impact by high-photospheric secondary motions is overestimated as it was mentioned above.

We compared MS-model averaged results for weak, moderate, and strong lines with observational ones by Hanslmeier et al. (1990). For comparison we used the theoretical data after smearing (spectral plus spatial smearing in frame of $SF3$). As is seen from a comparison of Table 3 with Table 4 the discrepancies between theoretical and observational correlations are not so large as in case of SS-models. So, MS-models are more close to the description of the real solar granulation.

Let us assume that the Paper I results have been selected subjectively and, for this reason, some observational correlations differ essentially from the statistical granulation data. But even in this case, we may hope that numerical modeling can reproduce the radiative-dynamic situations being similar to observations. Having such a goal, we analyzed the MS-model results and

Table 4. Comparison of the correlation coefficients from MS-model (Table 3) with the observational data of Hanslmeier et al (1990) for weak, moderate, and strong lines

Correlations	$Obs.$	$Cal.$	$Obs.$	$Cal.$	$Obs.$	$Cal.$
$<\delta i,\delta v>$	-0.56	-0.54	-0.45	-0.53	-0.18	-0.25
$error_{rms}$		0.015		0.015		0.019
$<\delta i,\delta EW>$	0.02	-0.06	0.31	0.04	0.12	0.09
$error_{rms}$		0.020		0.020		0.020
$<\delta v,\delta EW>$	0.06	0.19	-0.39	0.12	0.21	0.05
$error_{rms}$		0.020		0.021		0.022
$<\delta i,\delta r>$	0.52	0.85	-0.06	0.39	0.03	-0.30
$error_{rms}$		0.007		0.017		0.017

found several cases, when the modeled results were close to Paper I data. The sample of such cases becomes wide with decreasing spatial and spectral resolution and consist: Fe I 4911.54 Å – from 19 models without smoothing and 36 ones with the maximum value of the smearing; Fe I 4911.78 Å – from 4 cases and 29 ones, respectively. The basic peculiarity of selected MS-modeled spectral examples is a rather high positive correlation of $<\delta HW,\delta r>$ for weak and moderate lines and $<\delta v,\delta HW>$ is negative near -0.5. That means, the δHW enhancement lies between maximum and minimum Doppler velocities and δHW values correlate well with δr. Such a scenario of line parameter variations is not reproduced by SS-models. To understand the differences between selected MS-models and regular modeling we shall take two of them. We call their as $M1$ and $M2$. The line parameter correlation coefficients obtained with these models are represented in Table 5 and 6.

$M1$ and $M2$ models were selected in order to obtain the correlation coefficients similar to observational ones after allowing for the smearing effects. In Table 5 and 6 it is seen that for $M1$ and $M2$ models the differences between correlation coefficients for weak and moderate lines are not so strong as between averaged ones over all set of MS-models (Table 3). It is well seen that for weak and stronger lines the anticorrelations of $<\delta i,\delta v>$ and $<\delta v,\delta r>$ decrease, the positive correlation $<\delta i,\delta r>$ drops also. We should point out the increase of correlation between δHW and δr and anticorrelation between δEW and δr. The cause of such changes was discussed above.

5.1. Examples of artificial 2-D granulation: $M1$ model

The velocity distribution and isotherms of this model are shown in Fig. 5d. The dashed region in Fig. 5d is the area with Mach number (M) greater than 0.9 (maximum M is 1.5 in the photospheric layers and 3.0 in upper atmosphere). It is well seen that $M1$ differs from SS-models by inclined up- and downflows and by regions with supersonic velocities. They cause a break in the horizontal temperature distribution (shock), giving an additional perturbation to the velocity field. A possibility of forming horizontal flows with supersonic velocities was shown by Cattaneo et al. (1989) for 2-D polytropic models with high Re.

Table 5. Correlation coefficients and rms intensity fluctuations in continuum and line cores. *M1* model from set of MS-models

Correlations	$Without\ smearing$ 4911.8Å	$Smearing$ SF1 4911.8Å	$spectral+$ SF2 4911.8Å	$spatial$ SF3 4911.8Å	SF3 4911.5Å	SF3 6499.5Å
$<\delta i,\delta v>$	-0.92	-0.91	-0.84	-0.85	-0.86	-0.74
$<\delta v,\delta HW>$	0.41	0.09	-0.08	-0.23	-0.34	0.18
$<\delta v,\delta EW>$	-0.47	0.07	0.29	0.33	0.43	-0.10
$<\delta v,\delta r>$	-0.24	-0.81	-0.81	-0.83	-0.94	0.38
$<\delta i,\delta HW>$	-0.50	-0.36	-0.36	-0.19	-0.02	-0.24
$<\delta i,\delta EW>$	0.46	0.19	0.16	0.08	-0.04	0.51
$<\delta i,\delta r>$	0.27	0.64	0.52	0.57	0.88	-0.36
$<\delta HW,\delta EW>$	-0.15	-0.77	-0.89	-0.92	-0.95	-0.36
$<\delta HW,\delta r>$	0.22	0.40	0.57	0.68	0.44	0.71
$<\delta EW,\delta r>$	-0.54	-0.57	-0.72	-0.74	-0.50	-0.71
$\Delta I_{\rm rms}^{cont.},\%$	27.3	18.0	11.9	9.0	9.0	6.5
$\Delta I_{\rm rms}^{line},\%$	30.1	23.1	17.3	13.4	10.3	20.8

Table 6. Correlation coefficients and rms intensity fluctuations in continuum and line cores. *M2* model from set of MS-models

Correlations	$Without\ smearing$ 4911.5Å	$Smearing$ SF1 4911.5Å	$spectral+$ SF2 4911.5	$spatial$ SF3 4911.5Å	SF3 4911.8Å	SF3 6499.5
$<\delta i,\delta v>$	-0.79	-0.84	-0.79	-0.78	-0.74	-0.31
$<\delta v,\delta HW>$	0.35	0.23	-0.02	-0.36	-0.21	0.36
$<\delta v,\delta EW>$	0.19	0.50	0.55	0.61	0.55	0.70
$<\delta v,\delta r>$	-0.80	-0.93	-0.94	-0.94	-0.93	-0.43
$<\delta i,\delta HW>$	-0.43	-0.58	-0.45	-0.18	-0.35	-0.63
$<\delta i,\delta EW>$	0.02	-0.13	-0.09	-0.15	-0.02	0.21
$<\delta i,\delta r>$	0.93	0.93	0.91	0.90	0.64	-0.52
$<\delta HW,\delta EW>$	-0.22	-0.37	-0.47	-0.62	-0.52	0.20
$<\delta HW,\delta r>$	-0.24	-0.32	-0.10	0.21	0.40	0.48
$<\delta EW,\delta r>$	-0.28	-0.44	-0.45	-0.51	-0.69	-0.74
$\Delta I_{\rm rms}^{cont.},\%$	27.5	15.6	10.7	7.7	7.7	5.5
$\Delta I_{\rm rms}^{line},\%$	26.8	16.1	11.2	8.6	10.3	13.2

Note that the computational method of MS-models and spatial grid for modeling does not allow us to study this phenomenon with high precision. But we can make some conclusion concerning the occurrence of supersonic horizontal velocities in approximately real solar conditions. From the time-dependent set of MS-models (529 models, corresponding $\sim 4^h\ 24^m$) $\sim$ 55% (289 models) the horizontal flows with $M > 0.9$ occur. From this statistics we may conclude that in real conditions of the solar atmosphere these phenomena might be frequent enough and affect observational characteristics of the solar granulation.

Nesis et al. (1993) supposed that shocks, forming at granular border, can give the brightness increasing of granular border and enhance the nonthermal motions near those regions.

Let us consider such observational effects for the $M1$ model with the Fe I 4911.78 Å line computed (Figs. 6 and 5a–c). It can be seen from Fig. 6e, that the presence of shocks enhances the brightness at granular borders. But such a brightness is affected by increased upflows near granular border and deformation of the structure of downflows caused by supersonic flows. However, we do not see a drastic increase of HW above this region. The HW enhancement lies above the downflows. This is explained by the dependence of HW growth on the line-of-sight velocity gradient in the line forming region. We calculated the differences of model vertical velocities between model layers of $\log\tau_l^c = -1.5...-1.2$ (the line core forming region) and $\log\tau_l^c = -0.6...1.0$ (the forming region of line wings). Here τ_l^c is a sum of the optical depths in core and continuum.

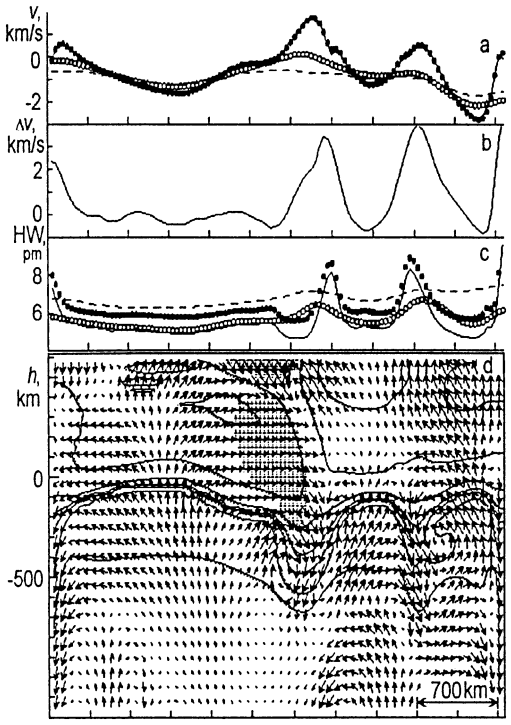

Fig. 5a–d. Moderate Fe I 4911.78 Å line: variations of velocities and line halfwidths (top). $M1$ multi-scale model (bottom). **a** Doppler velocities variations (δv). Designations correspond to Fig. 1b. **b** The difference of averaged model vertical velocities between layers which correspond the line core forming level and the forming level of line wings. **c** Line halfwidths variations (δHW). Designations correspond to Fig. 1b. **d** $M1$ model. Solid lines are isotherms for: 4000, 5000, 6000, 7000, 8000, 10000, and 12000 K (from top to bottom). The Mach in dashed region is more than 0.9.

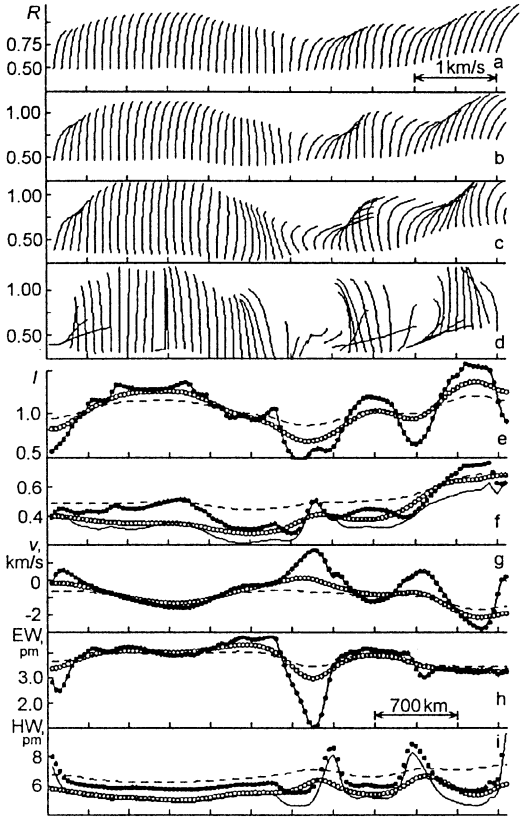

Fig. 6a–i. Moderate Fe I 4911.78 Å line: the line parameter variations for $M1$ model (Fig. 5d). Designations and plotting order correspond to Fig. 2.

The computed ΔV are represented in Fig. 5b and they are very close to HW variations (Fig. 5c) in fact.

We would like to note that as a result of impact by supersonic flows, it is also possible to create areas with inverse vertical distribution of the temperature. In this case, the central depths of the spectral lines decrease, their EW and HW drop and the Doppler velocities become more redshifted. As s result, the HW enhancement does not coincide with the maximum of decreasing velocities (Fig. 6). Additionally, the high horizontal velocities can impact onto the velocity field of nearest granules (Fig. 5d) leading to an inclination of the up- and downflows and decorrelate δHW and δv.

Line bisectors, obtained without any smoothing, show the direction of the moving matter. However, after spatial smearing, the lines which have the widest profiles bring the largest contribution into the resulting line profile. In most cases, these are the lines formed above downflows with the red asymmetry and the resulting smoothed profiles have got the red asymmetry in far wings. But above the shock we see a situation where the spectral lines have blue asymmetry in case allowing for the smearing (Fig. 6). As an important peculiarity of the bisector shape behaviour we may point the change of the bisector inclination above the shock region from blue to red.

5.2. Examples of artificial 2-D granulation: $M2$ model

The velocity field and isotherms are shown for this model in Fig. 7d. The parameter variations of the line Fe I 4911.54 Å are plotted in Fig. 7a–c and Fig. 8. In these models there are strongly inclined downflows at the center of the model. There is also the region with supersonic velocities (dashed region in Fig. 7d; the maximum M = 1.3 is in the photospheric layers, in the upper atmosphere – 3.4). They also break the temperature distribution. By their influence, the photometric profile of the granule is strongly deformed and becomes non-symmetrical (Fig. 8e). The Doppler velocities show a drastic break as a result of the presence of inclined up- and downflows which move with opposite direction. The peaks of HW cover the areas above downflows and reflect the gradients of line-of-sight velocities (in our case – vertical velocities). After spatial smearing, the Doppler velocities smear and HW maximum lies between maximum and minimum of Doppler velocities (Fig. 7c and 7a or Fig. 8i and 8g).

The behaviour of the bisectors are of special interest (Fig. 8d). But after spatial smearing the shape of bisectors drastically changes (Fig. 8a–c). The asymmetry of the lines, formed above downflows in the right part of the modeling region, becomes blue, while above the granule – red. I.e., it is opposite to that calculated directly from the models. We may note the same

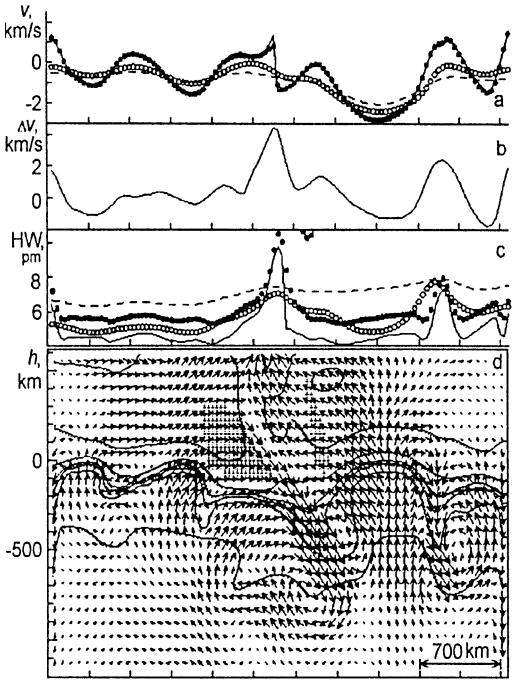

Fig. 7a–d. Weak Fe I 4911.54 Å line: variations of velocities and line halfwidths (top). $M2$ multi-scale model (bottom). Designations and plotting order correspond to Fig. 5.

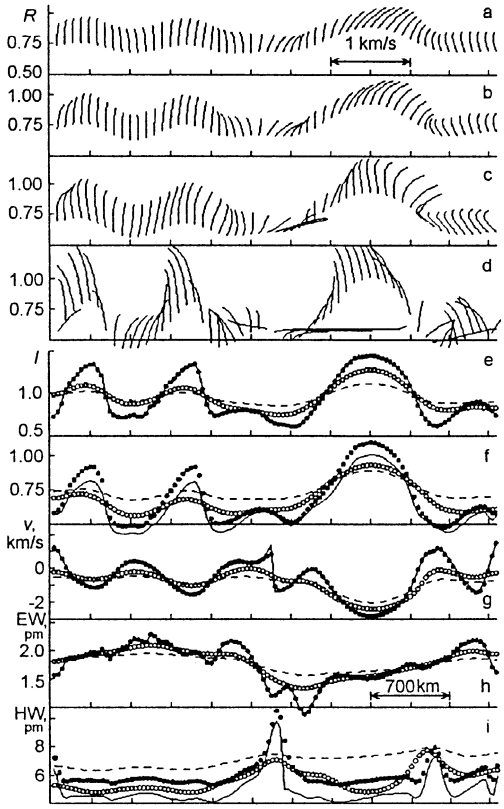

Fig. 8a–i. Weak Fe I 4911.54 Å line: the line parameter variations for $M2$ model (Fig. 7d). Designations and plotting order correspond to Fig. 2.

behaviour of the bisector shape above the shock region as in the case of $M1$.

6. Comparison with observations and discussion

Below we consider the main results of the MS-model study and compare them with observational data (Paper I; Nesis et al. 1992; Nesis et al. 1993). The conclusions will be done for Fe I 4911.54 and 4911.78 Å lines. Our qualitative results are similar to those which were found by Solanki et al. (1996) for the solar disk center.

• The low correlations between line parameters show the strong influence of the secondary motions on the overshooting convection. The SS-models with high-laminar flows in photosphere show high line parameter correlations. We also found the high amplitudes for time-dependent correlations causing by model oscillations. Maybe, they are overestimated.

• The data of Paper I do not show the correlation between $< \delta i, \delta HW >$. The value for this correlation, obtained as a time average from the models, was negative and rather high – about 0.5. This means that the bulk of MS-models show the HW enhancement above regions with low continuum intensity. But we should point that some part of MS-models demonstrates the δi and δHW behaviour being similar to Paper I – the HW enhancement between brightness extremes.

We note that a wider statistics regarding δi and δHW variations has been obtained for Ni I 4912.03 Å (Nesis et al. 1992, Nesis et al. 1993). From this we cannot make a simple conclusion concerning the correlation δi and δHW. For instance,

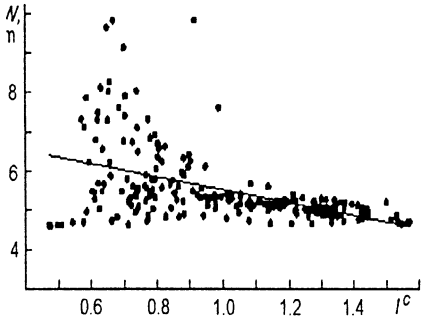

Fig. 9. Moderate 4911.78 Å line: the line halfwidths as a function of continuum intensity for $M1$ and $M2$ models.

from the 9 observational pictures given by Nesis et al. (1993) in about 3–4 cases the HW enhancement cover the low brightness areas. Moreover, in the paper of Nesis et al. (1992) the dependence of HW values on the continuum intensity is given. From this dependence the conclusion can be reached that the largest HW values are observed in regions with the lowest brightness.

In Fig. 9 we give theoretical dependencies of HW on continuum level intensity for the $M1$ and $M2$ models. It should be compared with the corresponding figures from the paper of Nesis et al. (1992). But such comparison may be qualitative only because Nesis et al. (1992) studied the Ni I 4912.03 Å line. As

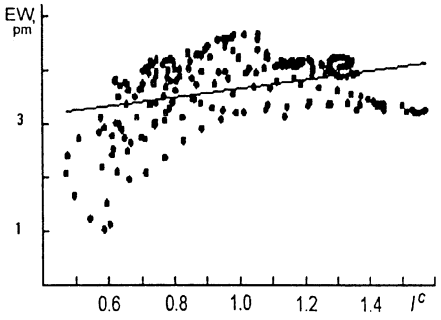

Fig. 10. Moderate 4911.78 Å line: the line equivalent widths as a function of continuum intensity for $M1$ and $M2$ models.

it is seen the behaviour of the theoretical values are very similar to the observational values.

• From observations (Paper I, Nesis et al. 1993, Karpinsky 1990) it follows that the brightest and darkest regions of the photometric granulation field not always coincide with corresponding largest up- and downflows. MS-models do not contradict this conclusion and it is confirmed by the low $< \delta i, \delta v >$ correlation. One example may be found in Fig. 8.

• In Paper I the bulk of bisectors is blue. Red asymmetry is observed between minimum and maximum of intensity. As it follows from the present results, the line asymmetry points in the direction of plasma motion and, after allowing for the smearing effects, they strongly depend on the spatial resolution and the dynamic situation in the nearest areas. The line asymmetry may reverse its shape. So, the results of analysis of observing bisectors should be interpreted with caution. However, in any case the bulk of blue or red bisectors reflects the essential influence of up- or downflows at (or near) the investigated region. If we consider the bisector shapes, obtained directly from models without any smoothing, we find that most bisectors are blueshifted indeed, because the upflow area size is larger than the downflow one.

• In Paper I the largest velocity gradients are found for high δHW values. That is confirmed by theoretical modeling.

• In Paper I it is noted that there is "a weak tendency of higher δEW values in darker areas" (Paper I). This conclusion seems to be open to discussion. It was obtained using one selected granule example for Fe I 4911.54 Å and an other picture for 4911.78 Å. Two another examples for line of Fe I 4911.78 Å demonstrate the alternative EW variations: in dark areas the lines with the less EW are observed. The similar result was found by Nesis et al. (1992) studying the observations of Ni I 4912.03 Å. The model predictions are in closer agreement to such results.

This is well seen in Fig. 10 where the EW values vs. continuum intensity for $M1$ and $M2$ models are shown.

• Paper I results do not give the essential differences between the parameter variations of weak (Fe I 4911.54 Å) and moderate (Fe I 4911.78 Å) lines. The similar results were obtained for SS-models with laminar overshooting convection. But averaged correlations show well the discrepancy between the data for weak and moderate lines, while for some MS-models such differences can be not so strong (Table 5 and 6). We already discussed this problem and suppose that it might be caused by an overestimation of the model secondary motions and by the slightly drowned overshooting convection.

• In Paper I the examples of "non-symmetrical variations of the line parameters around their maxima or minima" were shown. As it follows from numerical modeling, the symmetrical or non-symmetrical behaviour of line parameter variations depends on the flow topology, dynamic situation at the nearest regions, and preceding evolution. After taking into consideration the spectral and spatial decrease caused by artificial Gaussian smearing functions the number of symmetrical cases increases.

• In Paper I the largest blue asymmetry was found in regions with the HW maximum. Theoretical predictions, in the most cases, give qualitatively another result – at HW maximum the line asymmetry is the largest indeed, but it is red. However, the part of MS-models (for instance, Fig. 8) show such a dynamic situation when the spectral lines with the largest HW have a blue asymmetry. In Paper I examples were also shown when the lines above the darkest regions had both the red and blue asymmetry and this we discussed for the $M2$ MS-model above.

• From observations the δr enhancement was found at region with the higher intensity. Above we discuss such δr variations in detailed form. Here we note only, that this result is in good agreement with the theoretical model data both for SS- and MS-models.

6.1. The problem of the shock detection

In the frame of the 2-D models used we cannot confirm the suggestion of Nesis et al. (1992) that the HW enhancement may be caused by transonic flows. However, these models can explain the increase of line widths between granules and intergranular lanes but such HW peak cover areas not above the shock regions. They can be found at the border of the nearest granule as a result of impact of supersonic velocities onto nearest radiative dynamic situations. The shock can change the inclinations of flows, temperature distributions and photometric profile of granules.

We should note, there is a very special behaviour of spectral line bisectors above the shock region. Due to the impact from supersonic motions, the bisectors above this region change their own shape from blue to red over a small area. Such peculiarity is obvious from theoretical examples of the solar granulation and observed in the real field of the solar granulation (see, for instance, Paper I).

7. Conclusions

We see as the main results of the present paper the following:

• 2-D models of the solar granulation describing the convective motions as a quasi-stationary, cellular, and laminar system of quasi vertical velocity columns show high correlation values between variations of the line parameters and cannot explain the observational behaviour of spectral line characteristics over granular and intergranular areas.

• Better agreement with observed parameters can be obtained with the 2-D models which treat the solar thermal convection as fully non-stationary by a system of interacting flows. In these models the secondary motions play a very important role in the middle and upper model photosphere. As essential perturbing factors photospheric flows with supersonic velocities appear. They can change the photometric profiles of granules, can create the regions with inverse temperature distribution, impact onto the velocity field.

• Variations of line parameters strongly depend on limitation in spatial resolution (spatial smearing). To a largest degree this was found for variations of equivalent widths, full widths at half maxima, and bisectors of the lines.

Acknowledgements. A. Gadun and K. Pikalov are grateful to European Southern Observatory for the support of this work (Grant A-07-018). A. Hanslmeier thanks the Austrian Fonds zur Förderung der Wissenschaftl. Forschung (Proj. Nr. 10748). The authors thank the Austrian and the Ukrainian Academy of Sciences for financing the exchange of scientists.

References

Atroshchenko I.N., Gadun A.S., 1994, A&A 291, 635
Cattaneo F., Hurlburt N.E., Toomre J., 1989, Two and three-dimensional simulations of compressible convection. In: Rutten R.J. and Severino G. (eds.) Solar and Stellar Granulation, Kluwer, Dordrecht, p. 415
Delbouille L., Neven L., Roland G., 1973, Photometric Atlas of the Solar Spectrum from λ 3000 to λ 10000. Institut d'Astrophysique, Liège
Deubner F.L., Mattig W., 1975, A&A 45, 167
Gadun A.S., 1995, Kinemat. i Fiz. Nebesn. Tel 11, no. 3, 54
Gadun A.S., 1996, Kinemat. i Fiz. Nebesn. Tel 12, in press
Gadun A.S., Pikalov K.N., 1996, Solar Phys. 166, 43
Gadun A.S., Vorob'yov Yu.Yu., 1995, Solar Phys. 159, 45
Hanslmeier A., Mattig W., Nesis A., 1990, A&A 238, 354, PAPER I
Hanslmeier A., Mattig W., Nesis A., 1991, A&A 251, 669
Hanslmeier A., Mattig W., Nesis A., 1994, A&A 288, 960
Holweger H., Müller E.A., 1974, Solar Phys. 39, 19
Karpinsky V.N., 1990, Properties of the solar granulation. In: Stenflo J.O. (ed.) Solar Photosphere: Structure, Convection and Magnetic Fields. Kluwer, Dordrecht, p. 161
Kurucz R.L., 1979, ApJSS 40, no. 1, 1
Malagoli A., Cattaneo F., Brummel N.H., 1990, ApJ 361, L33
Markov V.S., 1991, Adv. Space Res. 11, no. 5, 215
Nesis A., Bogdan T.J., Cattaneo F., Hanslmeier A., Knölker M., Malagoli A., 1992, ApJ 399, L99
Nesis A., Hanslmeier A., Hammer R., Komm R., Mattig W., Staiger J., 1993, A&A 279, 599
Nordlund Å., 1984, Modelling of Small-Scale Dynamical Processes: Convection and Wave Generation. In: Keil S.L. (ed.) Small-Scale Dynamical Processes in Quiet Stellar Atmospheres, SPO, Sunspot, p. 174
Solanki S.K., Rüedi I., Bianda M., Steffen M., 1996, A&A 308, 623
Steffen M., 1989, Spectroscopic Properties of Solar Granulation Obtained from 2-D Numerical Simulations. In: Rutten R.J. and Severino G. (eds.) Solar and Stellar Granulation, Kluwer, Dordrecht, p. 425
Steffen M., Freytag B., 1991, Reviews of Modern Astron. 4, 43
Steffen, M., 1991, Stellar Atmospheres: Beyond Classical Models. In L. Crivellari et al. (eds.), Kluwer, NATO ASI Ser., 247
Stein, R.F., Nordlund, Å., 1989, ApJ 342, L95

This article was processed by the author using Springer-Verlag LaTeX A&A style file *L-AA* version 3.